Available online at www.sciencedirect.com
SCIENCE DIRECT®
Journal of Organometallic Chemistry 690 (2005) 84–95
Journal of Organometallic Chemistry
www.elsevier.com/locate/jorganchem

Theoretical study on interaction of different coordination modes of BH_4 ligand with transition metal in $[TM(BH_4)(CO)_4]^-$ (TM = Cr, Mo)

Alireza Ariafard [a,*], Mostafa M. Amini [b,*]

[a] Department of Chemistry, Islamic Azad University, Centeral Tehran Branch, Felestin square, Tehran, Iran
[b] Department of Chemistry, Shahid Beheshti University, Evin, Tehran, Iran

Received 27 January 2004; accepted 26 August 2004
Available online 25 September 2004

Abstract

Density functional calculations were performed on bonding and structural features of $[(\eta^n\text{-}BH_4)TM(CO)_4]^-$ ($n = 1, 2, 3$; TM = Cr, Mo) complexes. Calculations show that the ground state is bidentate which is in good agreement with experimental results. It has been found that the bridge and terminal hydrogen atoms will interchange by two pathways: (i) twist of BH_4 about one of the bridge B–H and (ii) twist of BH_4 about one of the terminal B–H. The molecular orbital calculations and natural bond orbital methodologies for different isomers of these complexes have been evaluated. The final results indicate that case (i) is more preferable relative to another case.

Keywords: Tetrahydroborate; Transition metal complexes; Chromium; Molybdenum; DFT calculation

1. Introduction

In recent decades, there has been considerable amount of interest in transition metal tetrahydroborato (BH_4) complexes. Several complexes have been synthesized and characterized by X-ray, neutron diffraction or by IR and NMR spectroscopies [1,2]. Besides their importance in homogenous catalysis, tetrahydroborates are of great interest due to the unusual coordination modes with transition metals through the η^1, η^2 and η^3 modes (Fig. 1). Most of these compounds contain metals in positive formal oxidation states [3,4].

Generally, the ^1H NMR spectra of metal tetrahydroborate complexes exhibit a single BH_4 resonance at room temperature. This situation has been reported regardless of whether the ground state metal tetrahydroborate coordination geometry is bidentate or tridentate, and this is due to the exceedingly rapid intramolecular interchange of bridge and terminal hydrogen atoms [5]. Various possible pathways have been proposed. The first pathway suggested stereochemical nonrigidity in tetrahydroborate complexes and involves permutation of bridge and terminal hydrogens via a monodentate intermediate or transition state [5] (Fig. 2).

Certain empirical observations as well as ab initio calculations [5–9] have suggested that, at least for the early transition metals, bidentate and tridentate structures do not differ much in energy. The second suggested pathway which is a concerted process for tetrahydroborates having bidentate reactant geometries twists the BH_4 ligand about

* Corresponding authors. Tel.: +98 21 4803708; fax: +98 281 2563931.
E-mail addresses: ariafard@yahoo.com (A. Ariafard), m-pourami-ni@cc.sbu.ac.ir (M.M. Amini).

0022-328X/$ - see front matter © 2004 Elsevier B.V. All rights reserved.
doi:10.1016/j.jorganchem.2004.08.034

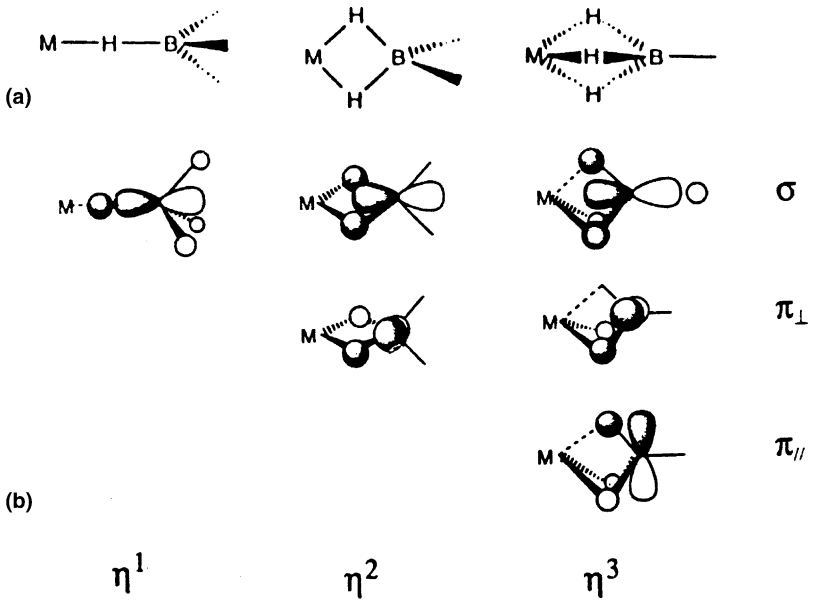

Fig. 1. (a) Three different coordination modes of BH_4. (b) BH_4 orbitals involve d orbitals in the η^1, η^2 and η^3 coordination modes.

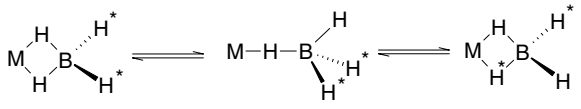

Fig. 2. Suggested pathway for interchange of bridge and terminal hydrogens through a monodentate intermediate or transition state.

one of the B–H^b bonds. The twisting process can be drawn for a complex with a tridentate reactant structure [5,10].

The aim of this work is to investigate the stability and possible structures of two examples of borohydride zero-valent metal complexes, $[Cr(CO)_4(BH_4)]^-$ [11] and $[Mo(CO)_4(BH_4)]^-$ [12] with the aid of density functional calculations. On the other hand, we have offered some insights into hydrogen exchange mechanism and also investigated relative stability of them through natural bonding orbital (NBO) and molecular orbital (MO) calculations.

2. Computational details

All geometries were fully optimized using the B3LYP (Becke three parameter exchange functional (B3) [13] and Lee–Yang–Parr correlation functional LYP [14]) density functional theory [15] as implemented in GAUSSIAN 98 [16]. In all tests the fine grid (75-302) was employed for a numerical evaluation of integrals. Mo and Cr atoms were described by effective core potentials (ECP's) of Wadt and Hay [17] with a double-ζ valance using the LANL2DZ. Carbons and oxygens are described with standard 6-31G basis set and polarization function is also added for carbon atoms, i.e., $\zeta_d(C) = 0.8$ [18]. The 6-31G** [19] is used for BH_4 ligand.

The natural bond orbital (NBO) analysis was performed using the NBO program [20] as implemented in GAUSSIAN 98. This program was also used to obtain Wiberg bond indexes (bond orders) [21], which is a measure of bond strength and occupancies. NBO occupancies were used to quantitatively evaluate the occupation number of given localized bonding orbitals, which give information regarding the strengths of interactions among different units within a molecule [22]. Frequency calculations were performed to determine the characteristics of optimized stationary geometries.

3. Results and discussion

The synthesis BH_4 adducts of $TM(CO)_4$ (TM = Cr, Mo) have been reported through a mixture of $PPN^+TM(CO)_5I^-$ with $PPN^+BH_4^-$ in THF [11,12]. Here, we focus on the structural isomers and bonding studies of the BH_4 adducts of $TM(CO)_4$ using the density functional theory (DFT) method as described in Section 2.

3.1. Effect of computational methods

The HF, DFT-B3LYP and MP2 fully optimized geometries of $[(\eta^2\text{-}BH_4)TM(CO)_4]^-$ (TM = Cr, Mo) (see 1) with C_{2v} symmetry are given in Tables 1 and 2. Frequency calculations of three methods showed no imaginary frequency for these complexes.

Table 1
Calculated geometry parameters (Å, °) for $(\eta^2\text{-}BH_4)Mo(CO)_4$ complex

Geometry parameters	HF	B3LYP	MP2	Exptl[a]
Mo–B	2.503	2.464	2.435	2.413
Mo–C_{eq}	2.020	1.978	1.953	1.935 av.
Mo–C_{ax}	2.108	2.053	2.033	2.036 av.
C–O (ax)	1.127	1.162	1.171	1.128 av.
C–O (eq)	1.139	1.173	1.186	1.157 av.
C_{ax}–Mo–C_{eq}	90.92	89.75	88.72	88.98 av.
C_{eq}–Mo–C_{eq}	91.04	90.22	85.58	84.50
C_{ax}–Mo–C_{ax}	177.37	179.28	176.5	176.70
Average deviation %	2.79	2.25	1.16	

[a] Ref. [12].

Table 2
Calculated geometry parameters (Å, °) for the $(\eta^2\text{-}BH_4)Cr(CO)_4$ complex

Geometry parameters	HF	B3LYP	MP2	Exptl[a]
Cr–B	2.369	2.286	2.232	2.29
Cr–C_{eq}	1.914	1.835	1.774	1.81 av
Cr–C_{ax}	1.984	1.889	1.836	1.86 av
C–O (ax)	1.126	1.163	1.177	1.15 av
C–O (eq)	1.136	1.172	1.192	1.16 av
C_{ax}–Cr–C_{eq}	91.80	89.69	87.45	88.57 av
C_{eq}–Cr–C_{eq}	96.50	93.93	83.12	94.8
C_{ax}–Cr–C_{ax}	174.65	179.26	173.18	175.6
Average deviation %	2.89	1.16	3.25	

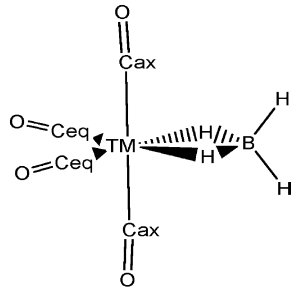

1

A comparison of the calculated geometrical parameters of η^2 structures obtained from above methods to experimental values is given in Tables 1 and 2. Because the $[Cr(CO)_4(BH_4)]^-$ [11] and $[Mo(CO)_4(BH_4)]^-$ [12] structures have been determined by X-ray diffraction, so the positions of the hydrogen atoms suffer from systematic error. Due to this systematic error, we have ignored structure parameters regarding the hydrogen atoms. Comparison to the experimental values, the overall average deviation at HF level for the Mo and Cr complexes are 2.79% and 2.89%, respectively, where the metal–ligand bond lengths are too long with this method. This difference can be attributed to the lack of electron correlation at HF level. The geometrical parameters that obtained from B3LYP and MP2 of Mo complex are in much better agreement with the X-ray structure data with average deviation of 2.25% and 1.16%, respectively. However, the MP2 optimized structure of Cr complex with average deviation 3.35%, is quantitatively different from B3LYP optimized ones. For the Cr complex, the largest difference between B3LYP and MP2 values are obtained for metal–ligand distance, which all are shorter at MP2 level. The short MP2 Cr–C and long MP2 C–O bond lengths indicate that the strength of the back-donation is exaggerated by the MP2 method.

Generally, first row transition metal complexes are significantly more difficult to treat with the HF and MP2 methods than second and third row transition metal complexes. The more compact character of 3d orbitals than 4s orbital is the major reason for this behavior [23]. The compactness of the 3d orbital leads to the presence of strong near-degeneracy effects, as a result of weak overlap between the 3d orbitals and ligand orbitals [24,25]. Because the 4d and 5d orbitals are significantly larger relative to 3d orbitals, the influence of near-degeneracy problems on the complexes of second- and third-row transition metals are smaller. Near-degeneracy problems often lead to multireference character in the state of interest, and in principle, these states cannot be described correctly by single-reference methods such as HF or MP2 [25]. A poor description of the electronic state by HF or MP2 may lead to incorrect results for the geometry optimization. DFT methods (in this study B3LYP) are efficient and accurate computational methods in studies of transition metal complexes, especially for treating complexes containing first row transition metals.

3.2. Molecular structures

The complete structures of fully optimized of $[(BH_4)TM(CO)_4]^-$ (TM = Cr, Mo) at DFT-B3LYP level are shown in Fig. 3. Selected bond distances and angles for these structures are given in Tables 3 and 4. The $[(\eta^2\text{-}BH_4)TM(CO)_4]^-$ isomer (**A**) has the lowest energy compared with the other structures, and it has only real vibrational frequencies. The majority of tetrahydroborate complexes obey the 18-electron rule when η^1, η^2 and η^3-BH_4 are considered to donate two, four or six electrons to the central metal [1]. Above-mentioned complexes also obey this rule, but species **B**–**F**, which do not obey 18 electron rule, are less stable than **A** (see Table 5). The isomer **A** has C_{2v} symmetry while the **B**–**F** structures have C_s symmetry.

In order to obtain η^3- and η^1-BH_4 structures, TM–B–H_t and TM–H_b–B bond angles were kept linear, respectively, because all attempt to constrain the bond angle to 180° with C_s symmetry resulted in return to isomers **B** and **E**.

The two pseudo-η^3 isomers (**C** and **D**) are related to each other by a 30° rotation of the borohydride ligand

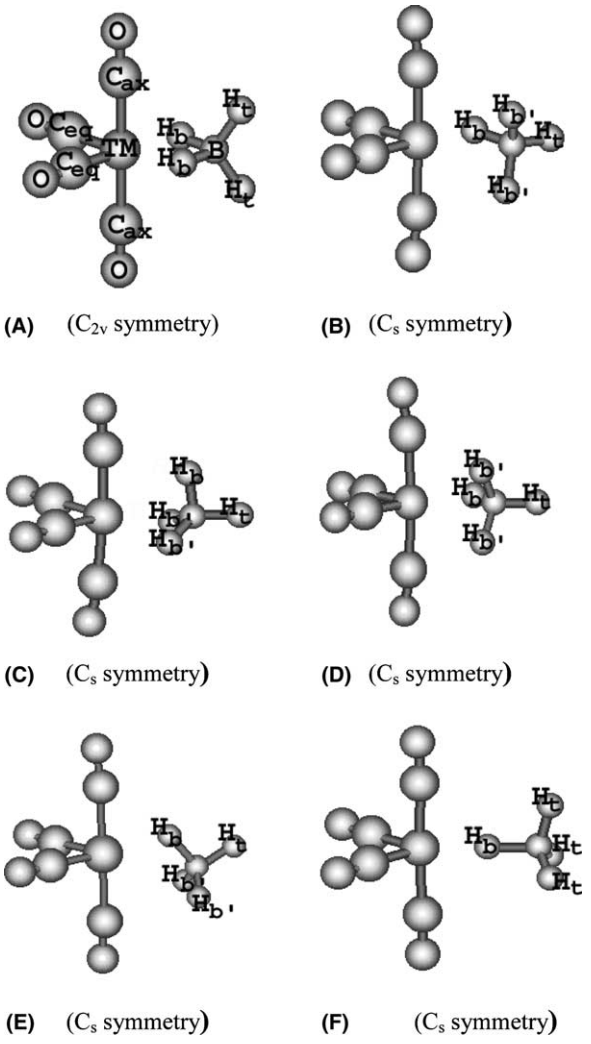

Fig. 3. Six different isomers for $[TM(CO)_4(BH_4)]^-$ (TM = Cr and Mo).

about B–TM axis. The study on 30° rotamer of the η^1 structure (**F**) showed that it is essentially identical in energy to **F**.

The computed energies (kcal/mol) of isomers **B**–**F** relative to the **A** along with their symmetries are given in Table 5. In both Cr and Mo complexes, the η^2 isomer (**A**) was found to be in the lowest energy. In both compounds, the isomers **B**–**E** were calculated to have almost close stability at the B3LYP level.

For all isomers, the vibrational frequencies have been numerically calculated at B3LYP level for the characterization of nature of stationary point. The number of imaginary frequencies are listed in Table 5. Though the vibrational frequency calculations for such non-stationary structures (**C**, **D** and **F**) are meaningless, the calculations at least indicate that the **C** and **F** with two and three imaginary frequencies could not be a transition state for exchanging the bridge H^b and terminal H^t hydrogen atoms. On the other hand, the frequency calculations reveal that **B**, **D** and **E** have only one imaginary frequency. For these isomers, imaginary frequencies correspond to the harmonic motions that would lead them to an η^2 isomer. As a result, **B** and **E** are undoubtedly transition states for exchange of H^b and H^t hydrogen atoms and **D** can be assumed as an imaginary transition state for comparing with real ones.

Experimentally, bridge-terminal hydride exchange in $[Cr(CO)_4(\eta^2\text{-}BH_4)]^-$ was found to be rapid at −80 °C [11], and ΔG for the $[Mo(CO)_4(\eta^2\text{-}BH_4)]^-$ was measured to be 10.0 ± 0.2 kcal/mol [12]. Our calculated barriers at B3LYP level are roughly consistent with values derived from experiment (see Table 5).

3.3. HOMO in pseudo-η^3 isomers

It should be noted that there is considerable asymmetry in the pseudo-η^3 bonding modes. In order to understand behavior of these isomers, we have plotted the metal–borohydride MO that corresponds to the highest occupied molecular orbital (HOMO) of **C** and **D**, as shown in Fig. 4. In **C**, TM–H_b bond is significantly longer than TM–$H_{b'}$ bonds, while in **D**, it is reversed (see Tables 3 and 4). These changes are essentially due to the antibonding interaction between metal and borohydride in the HOMOs. In isomer **D**, the HOMO represents metal–BH_4 $\pi^*_\perp$ (see Fig. 1) antibonding interaction,

Table 3
Selected bond distances (Å) and angles (°) in $[TM(CO)_4(BH_4)]^-$ (TM = **Cr**)

TM = Cr	$[TM(CO)_4(BH_4)]^-$					
	A	**B**	**C**	**D**	**E**	**F**
TM–B	2.285	2.441	2.233	2.364	2.696	3.042
TM–H_b	1.817	1.830	2.529	2.036	1.795	1.745
TM–$H_{b'}$	–	2.612	2.070	2.377	3.014	–
B–H_b	1.288	1.294	1.219	1.273	1.280	1.297
B–$H_{b'}$	–	1.219	1.257	1.224	1.219	–
B–H_t	1.210	1.213	1.210	1.210	1.219	1.214
TM–C_{ax}	1.889	1.899	1.906	1.905	1.884	1.895
TM–C_{eq}	1.835	1.816	1.826	1.819	1.824	1.825
C_{ax}–TM–C_{ax}	179.3	177.1	176.2	175.4	179.2	177.3
C_{eq}–TM–C_{eq}	93.9	92.4	92.8	92.6	91.4	91.2
C_{ax}–TM–C_{eq}	90.2	88.7	88.6	89.4	90.1	90.9

Table 4
Selected bond distances (Å) and angles (°) in $[TM(CO)_4(BH_4)]^-$ (TM = Mo)

TM = Mo	$[TM(CO)_4(BH_4)]^-$					
	A	**B**	**C**	**D**	**E**	**F**
TM–B	2.464	2.530	2.467	2.480	2.760	3.192
TM–H_b	1.991	2.010	2.579	2.185	1.975	1.891
TM–$H_{b'}$	–	2.633	2.232	2.453	3.006	–
B–H_b	1.287	1.294	1.217	1.273	1.273	1.301
B–$H_{b'}$	–	1.222	1.258	1.226	1.222	–
B–H_t	1.209	1.210	1.208	1.208	1.216	1.213
TM–C_{ax}	2.053	2.059	2.065	2.062	2.046	2.057
TM–C_{eq}	1.978	1.945	1.959	1.951	1.953	1.954
C_{ax}–TM–C_{ax}	179.3	176.0	175.0	174.4	179.0	179.1
C_{eq}–TM–C_{eq}	88.9	88.9	88.8	88.7	87.8	87.7
C_{ax}–TM–C_{eq}	88.0	88.0	87.9	87.4	89.3	90.3

Table 5
Symmetries, number of imaginary frequencies and relative energies for $[TM(CO)_4(BH_4)]^-$ (TM = Cr, Mo)

Species	Number of imaginary frequencies	Symmetry	Relative energy for Cr complex (kcal/mol)	Relative energy for Mo complex (kcal/mol)
A	0	C_{2v}	0	0
B	1	C_s	15.6	13.1
C	2	C_s	19.4	15.0
D	1	C_s	20.1	15.4
E	1	C_s	20.6	18.4
F	3	C_s	22.7	21.4

therefore, $H_{b'}$ atoms in this structure slide away from the central metal relative to H_b (see Fig. 4(a)). Furthermore, in isomer **C**, the HOMO has $\pi^*_{\|}$ characteristic (see Fig. 1), so repulsion between H_b and central metal orbitals causes an increase in metal–H_b bond distance (see Fig. 4(b)). What occurs in **C** is a rocking motion, which causes the TM–H_b distances to become longer than TM–$H_{b'}$. For **D** the rocking motion occurs out of the plane of paper. Therefore, one expects that these changes lead to a decrease in the net repulsion between transition metal and BH_4.

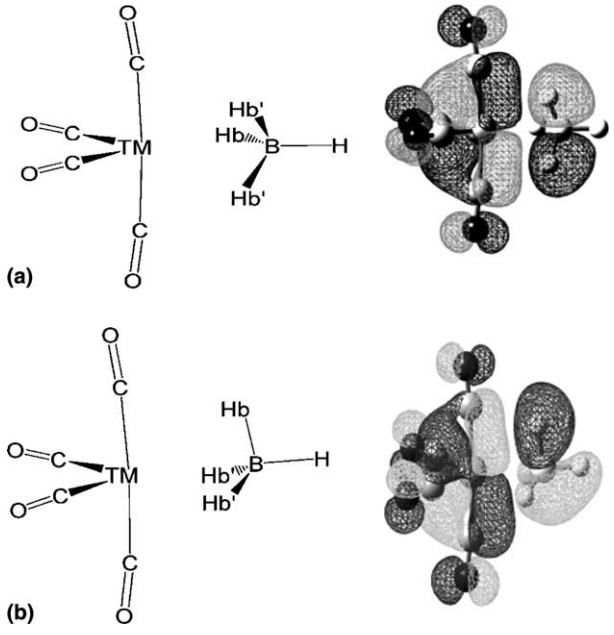

Fig. 4. (a) Spatial plot of the HOMO for **D**. (b) Spatial plot of the HOMO for **C**. The molecular orbitals were obtained from the B3LYP calculations.

3.4. Isomers *B* and *E*

Interestingly, we can find that transition states **B** and **E** correspond to two different twisting modes for BH_4 ligand about one of the B–H bonds of BH_4 ligand. In the first case BH_4 is twisting about one of the B–H^b bonds (**B**) and in the second case it is twisting about one of the B–H^t bonds (**E**) (Fig. 5).

An question can immediately be arised. What would coordination mode of BH_4 be in these isomers, η^3 or η^1? In this section, we attempt to answer this question. It must be realized that in each one of coordination modes, η^1, η^2, and η^3, each B–H–TM linkage can be viewed as a three center-two-electron bond. MO analyses of mono-tetrahydroborate complexes showed that each BH_4 ligand, as mentioned above, can acts as a two, four, or six electron donor in the η^1, η^2, η^3 coordination modes, respectively [26,27]. In other words, each B–H unit donates its σ-bonding electron pair to metal center to form a metal–ligand dative bond. Complexes with these characteristics of bonding are also called σ-complexes [28]. In these isomers, the B–$H_{b'}$ bond distances calculated in the BH_4 units are in the rang observed for B–H^t bonds. The shorter B–$H_{b'}$ distances suggest that these bonds are terminal (see Tables 3 and 4). Tables 3 and 4 clearly show that the B–$H_{b'}$ distances of these complexes are within 1.190–1.222 Å, while those of B–H_b bonds are 1.273–1.295 Å. In isomers **B** and **E**, the shortening of the B–$H_{b'}$ distances is an indication of decrease in the donoring ability of B–$H_{b'}$ σ orbital to

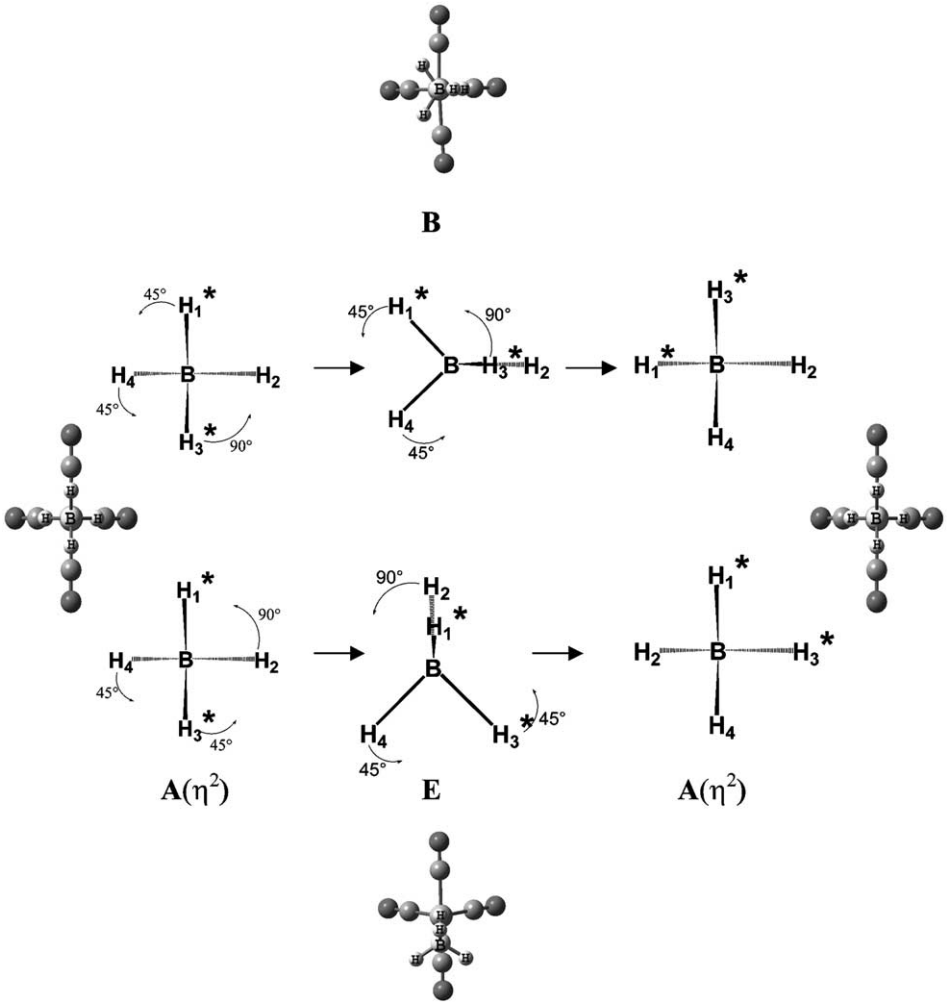

Fig. 5. Suggested pathway for interchange of bridge and terminal hydrogens through BH_4 twisting about one of bonds: (a) B–H_b (isomer **B**); (b) B–H_t (isomer **E**). In the chemdraw structures the metal fragment is omitted for clarity.

the central metal. For further elucidation regarding BH_4 coordination mode in these isomers, we also used NBO analysis. For isomers **B** and **E** the NBO analyses show that occupation numbers of B–H_b bonds are within 1.74–1.77, while those of B–$H_{b'}$ are 1.94–1.96 (see Table 6). In addition, in **B** and **E**, one can find that the TM–$H_{b'}$ bond distances are significantly longer than TM–H_b bond distances. The corresponding bond indices, listed in Table 7, also show a similar trend. Table 7 indicates that in **B** and **E** TM–$H_{b'}$ Wiberg bond indices are very small and by examining the results of calculations, it seems that in **B** and **E**, BH_4 ligand is in the η^1 coordination mode.

3.4.1. BH_4 vibrational frequencies of *B* and *E*

The different bonding modes of tetrahydroborate give rise to distinct and characteristic patterns of vibrational frequencies [29]. The experimental observations indicate that, a triply bridged group with C_{3v} local symmetry has three stretching modes, one of terminal bond (a mode) and two of bridge bonds (a and e modes), at 2450–2600 and 2100–2200 cm^{-1}, respectively, while a singly

Table 6
Natural bond orbital occupancies for the BH_4 ligand of the $[TM(CO)_4(BH_4)]^-$ complexes

	TM = Cr			TM = Mo		
	A	**B**	**E**	**A**	**B**	**E**
B–H_b	1.72	1.74	1.77	1.76	1.76	1.80
B–$H_{b'}$	–	1.96	1.98	–	1.94	1.97
B–H_t	1.99	1.97	1.96	1.99	1.98	1.97

Table 7
The calculated Wiberg bond indices for the TM–H bonds of the $[TM(CO)_4(BH_4)]^-$ complexes

	TM = Cr			TM = Mo		
	A	**B**	**E**	**A**	**B**	**E**
TM–H_b	0.141	0.138	0.126	0.133	0.132	0.126
TM–$H_{b'}$	–	0.023	0.012	–	0.028	0.018
TM–H_t	0.004	0.016	0.017	0.003	0.016	0.010

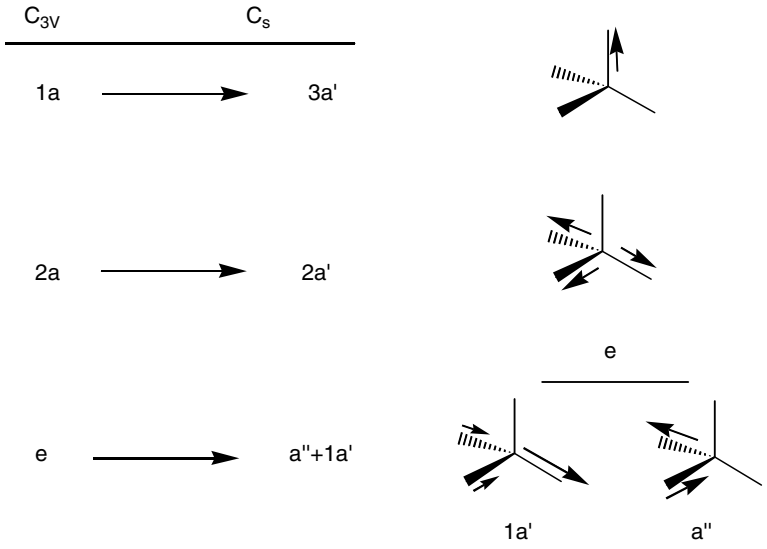

Fig. 6. The B–H stretching modes of BH_4 ligand with C_{3v} local symmetry and the reduced modes to C_s symmetry.

bridged group, also with C_{3v} symmetry, has three stretching mode, two of terminal bonds (a and e modes) and one of bridge bond (a mode), at 2300–2450 and ca. 2000 cm^{-1} [29]. These observations prompted us to calculate the vibrational frequencies of **B** and **E** at B3LYP level to predicate appropriate coordination mode for these structures.

Fig. 6 shows reduction of BH_4 stretching modes from C_{3v} to C_s symmetry. As shown in this figure, we can obtain 1a′ and a″ modes by decreasing of e mode, from C_{3v} to C_s symmetry, therefore, four vibrational frequencies for BH_4 ligand in a structure with C_s symmetry is predicated. Since the isomers **B** and **E** have C_s symmetry, the BH_4 stretching modes of these isomers correspond to

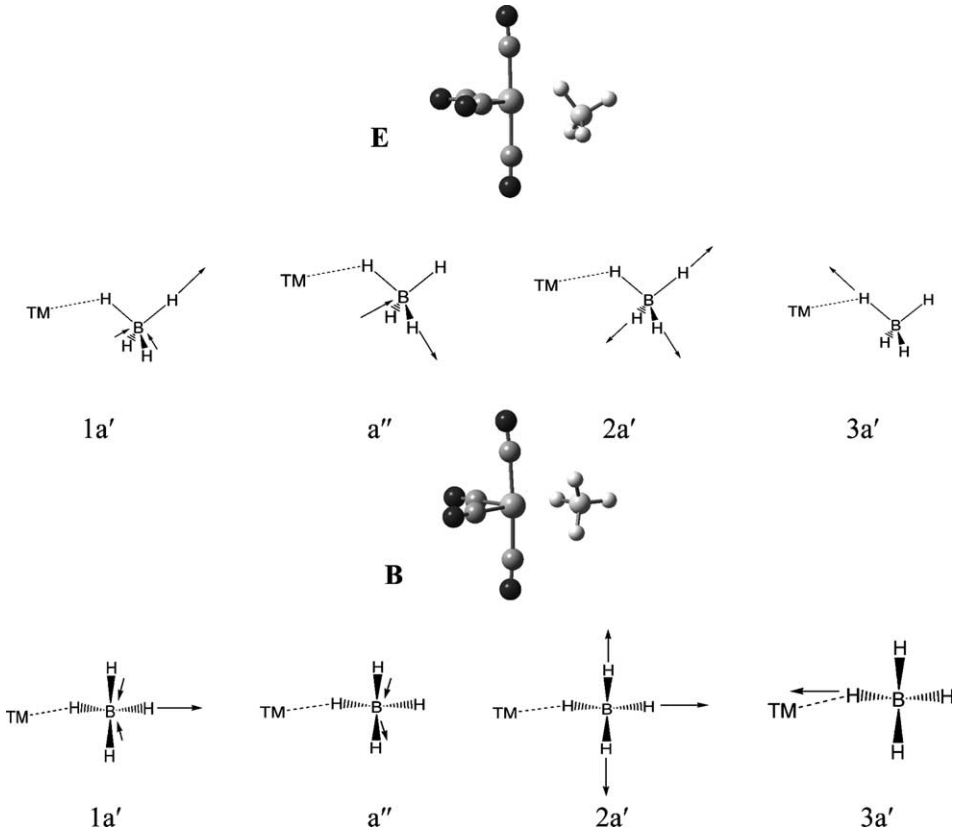

Fig. 7. Stretching modes of BH_4 ligand in isomers **B** and **E**.

Table 8
Energy value (cm^{-1}) of different stretching modes of B–H in isomers B and E for Mo and Cr complexes

Species	Isomers	1a′	a″	2a′	3a′
$[Cr(BH_4)(CO)_4]^-$	**B**	2483.2	2422.1	2403.8	1961.7
	E	2446.9	2432.5	2404.3	2111.3
$[Mo(BH_4)(CO)_4]^-$	**B**	2505.1	2409.5	2395.0	1956.7
	E	2460.8	2412.6	2394.6	2099.8

1a′, 2a′, 3a′ and a″ (Fig. 7). The calculated frequencies of the various modes of BH_4 stretches for these two structures and also symmetry of relevant vibrational patterns of them are shown in Table 8. The frequencies do not change significantly with the metal ion and coordination type. They vary from 2394 to 2505 cm^{-1} in the modes of 1a′, 2a′ and a″ and from 1956 to 2111 cm^{-1} in a case with 3a′ mode. Therefore, one can easily find that these vibrational frequencies are characteristic of the BH_4 stretching modes for a η^1 coordination mode.

3.5. Charge transfer

The NBO analysis was also carried out at B3LYP level to estimate the charge transferred between the metal center and BH_4 ligand in the formation of tetrahydroborate complex. Configuration of the TM atoms and natural atomic charge of the most stable conformation and transition states (**B**, **D** and **E**) have been evaluated by the natural population analysis, and they are presented in Table 9. In all isomers studied here, the charge is transferred from BH_4 ligand (which is the electron donor through σ-bonding electron pair of B–H) to central metal, but also the CO ligands receive part of this charge. Examining each isomer structure separately, we found that the charge transferred is larger for the most stable conformation. The overall charge on the BH_4 fragment suggests that for the transition structures less charge is transferred to $TM(CO)_4$, therefore, the TM negative charge becomes smaller. Furthermore, the extent of charge transfer suggests that the ionic properties increase from the most stable conformation to the transition states. The analysis of the dipole moment of these complexes confirms the greater ionic nature of the transition states (Table 10). It is also interesting to note that while TM nd orbitals population varies among the four isomers and decreases from **A** to **B = D** and then to **E** isomers, the TM $(n+1)$s orbital population remains essentially constant (about 0.4 $|e^-|$). This suggests that the d orbitals are significantly involved in the BH_4 bonding to central metal.

3.6. Molecular orbital calculation

For isomers **A**, **B** and **E**, inspection of lowest unoccupied molecular orbital (LUMO) and also three orbitals that accommodate the six d electrons correspond to the three HOMOs are shown in Fig. 8. The HOMOs for **A** mainly represent the TM–BH_4 nonbonding interaction. In other isomers, the HOMO-1 and HOMO-2 also show TM–BH_4 nonbonding interaction, whereas the HOMO to some extent has TM–BH_4 π-antibonding interaction. In isomer **A**, the HOMO, HOMO-1 and HOMO-2 are mainly d_{xy}, d_-, and d_+ orbitals, respec-

Table 9
Natural population analysis for the most stable conformation and the transition state structures in the B3LYP level, and the charge average values for CO groups in the equatorial and axial positions

Isomer structure	$[TM(CO)_4(BH_4)]^-$									
	TM = Cr					TM = Mo				
	Charge				Conformation of TM	Charge				Conformation of TM
	BH_4	$(CO)_{ax}$	$(CO)_{eq}$	TM		BH_4	$(CO)_{ax}$	$(CO)_{eq}$	TM	
A	−0.499	0.314	0.212	−1.059	$4S^{0.42}\ 3d^{6.62}$	−0.536	0.176	0.064	−0.703	$5s^{0.39}\ 4d^{6.32}$
B	−0.648	0.278	0.160	−0.789	$4s^{0.4}\ 3d^{6.37}$	−0.665	0.160	0.032	−0.533	$5s^{0.38}\ 4d^{6.18}$
D	−0.684	0.268	0.162	−0.760	$4s^{0.39}\ d^{6.37}$	−0.685	0.158	0.053	−0.545	$5s^{0.37}\ 4d^{6.18}$
E	−0.719	0.271	0.116	−0.666	$4s^{0.41}\ 3d^{6.26}$	−0.739	0153	−0.020	−0.391	$5s^{0.39}\ 4d^{6.03}$

Table 10
Calculated dipole moment for isomers **A**, **B**, **D** and **E**

Isomer	$[TM(CO)_4(BH_4)]^-$							
	TM = Cr				TM = Mo			
	A	**B**	**D**	**E**	**A**	**B**	**D**	**E**
Dipole moment (Debye)	2.55	3.44	3.18	4.56	2.69	3.13	2.59	4.34

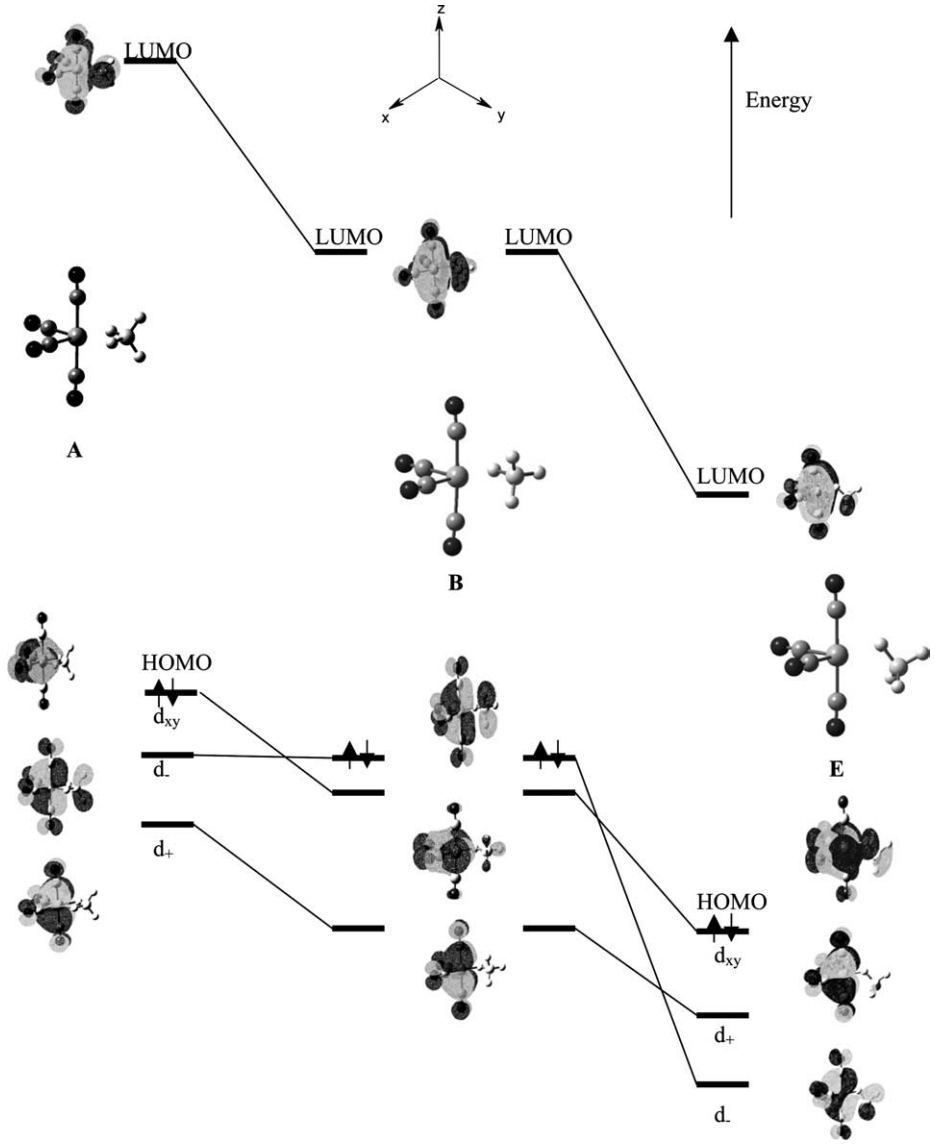

Fig. 8. Schematic orbital correlation diagram showing the three highest occupied molecular orbitals and the lowest unoccupied molecular orbital for isomes **A**, **B**, and **E**.

tively. The d_+ orbital represents the linear combination of $d_{xz} + d_{yz}$, while the d_- orbital represents $d_{xz} - d_{yz}$. In all isomers, the LUMO is of TM–BH_4 π-antibonding interaction. These calculations show that the major changes are the rise in the energy level of the LUMO, which increase in the order of **A** > **B** > **E** (see Table 11 and Fig. 8). As mentioned above, the analysis of NPA charges (Table 9) indicates that the BH_4 fragment has greater charge in the isomers **E** and **B**, thus, it suggests that less charge is transferred to $TM(CO)_4$ fragment compared with the most stable conformation (**A**). These results indicate that σ-bonding donation of B–H bonds and also covalent nature of these isomer structures increase in the order of **A** > **B** > **E**. It can also be concluded that the high stability of the **B** compared with **E** is mainly caused by σ-donation of B–H bonds. In other words, the better charge transfer of BH_4 ligand in isomer **B** shifts the energy level of the LUMO more upward than isomer **E**, therefore, it is clear that BH_4 in isomer **B** is a better σ-donor. The stability of these structures also supports from larger the HOMO–LUMO gap in which the maximum differences of this gap belong to ground state (**A**), having more stability than other isomers. In **B**, this difference is less than that of **E**.

Evaluation of MOs of isomer **D** gives results similar to those of **B** (Fig. 9). Examining Tables 9 and 11, we found that for **B** and **D**, the extent of charge transfer and the HOMO–LUMO gap are almost same. In contrast to these results, **B** by 4.5 kcal/mol in Cr complex and by 2.5 kcal/mol in Mo complex is more stable than **D**. Based on the HOMO antibonding character, one can

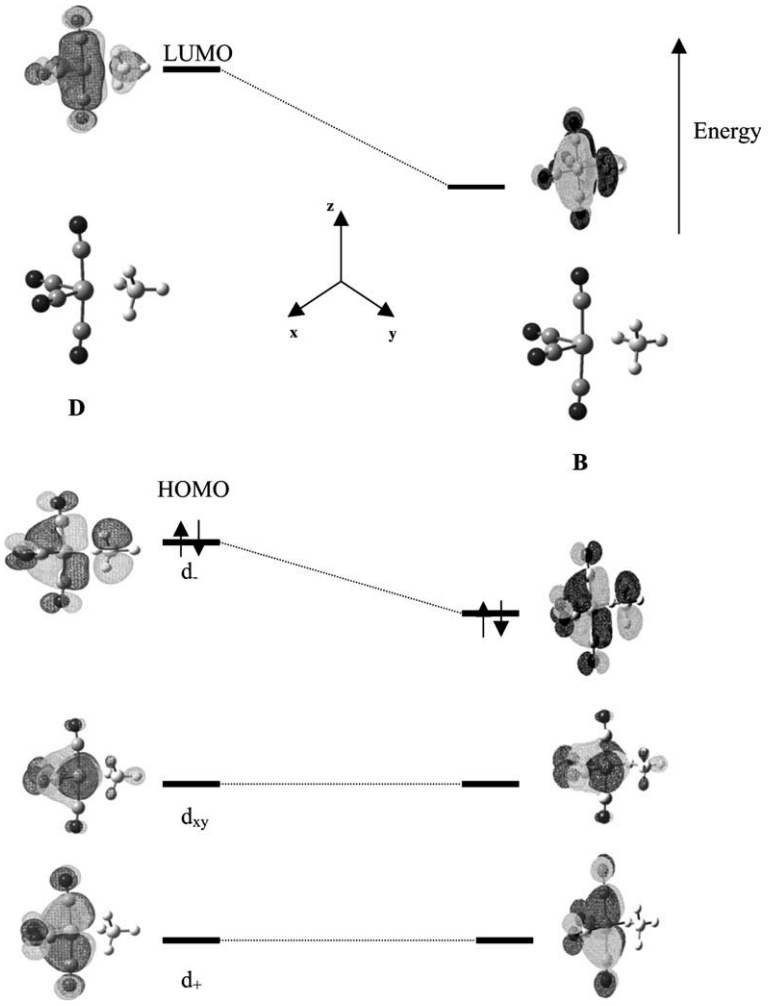

Fig. 9. Schematic orbital correlation diagram showing the three highest occupied molecular orbitals and the lowest unoccupied molecular orbital for isomers **B** and **D**.

understand the reason for higher stability of **B** in comparison with **D** (see Fig. 9). Since in isomer **D**, $H_{b'}$ atoms are closer to TM (2.377 and 2.453 Å in Cr and Mo complexes) in comparison with those of isomer **B** (2.612 and 2.633 Å in Cr and Mo complexes), we expect that, in **D**, TM–BH_4 π-antibonding interaction would be more significant than that of **B**, which causes HOMO of **D** become unstable compared with that of **B**. This behavior would rationalize high stability of isomer **B** with respect to **D**.

In these isomers, the increase of σ-donation of BH_4 ligand can also enhance the energy level of nonbonding d orbitals, e.g., energy level of d_+, which is a nonbonding orbital, increases in the order of **A** > **B** = **D** > **E**.

Interestingly, the results of calculations indicate that the Cr isomers need higher energies for hydrogens exchange in comparison with the Mo isomers (Table 5). The results derived from the amount of charge transfer (Table 9) and the HOMO–LUMO gap (Table 11) of isomer **A** of both Mo and Cr complexes suggest that chromium has stronger bonding interactions with BH_4 ligand, stabilizing the stable species more than the transition state species.

3.7. Mechanism of bridge-terminal hydrogens exchange

The structures of the most stable conformation and the transition states allowed us to evaluate important thermodynamic activation parameter, namely the activation volume ($\Delta V^{\ddagger}$). This quantity is certainly interesting in defining the nature of a substitution reaction, i.e., if the mechanism is dissosiative, D, assosiative, A, interchange-dissosiative, I_d, or interchange-assosiative, I_a. For tetrahydroborate transition metal complexes, in general, both A and D mechanisms for exchange of hydrogen are ruled out experimentally and instead intramolecular reactions have been suggested [29,30]. In order to compute the activation volume, we decided to evaluate the volume of the most stable isomer and transition state species, as proportional to the sum of all

Table 11
Orbital energies (a.u.) of HOMOs, LUMO and HOMO–LUMO gap of transition states for Mo and Cr complexes

Arrangement	$[TM(CO)_4(BH_4)]^-$							
	TM = Cr				TM = Mo			
	A	**B**	**D**	**E**	**A**	**B**	**D**	**E**
HOMO-2	−0.075	−0.081	−0.081	−0.091	−0.083	−0.087	−0.087	−0.093
HOMO-1	−0.075	−0.076	−0.076	−0.090	−0.081	−0.076	−0.076	−0.091
HOMO	−0.070	−0.073	−0.064	−0.079	−0.072	−0.075	−0.068	−0.079
LUMO	0.082	0.062	0.070	0.045	0.069	0.059	0.064	0.045
HOMO–LUMO gap	0.152	0.135	0.134	0.124	0.141	0.134	0.132	0.124

Table 12
Calculated Σ_{Y-A} (Å) in both Cr and Mo complexes

Complex	Σ_{B-A}	Σ_{D-A}	Σ_{E-A}
Cr	0.901	0.580	1.993
Mo	0.475	0.254	1.501

metal to donor atom distances as previously applied to similar substitution reaction [31,32]. According to this study the activation volume is the difference between the transition state and the most stable isomer volumes, which is proportional to Σ, estimated by following equation [31,32]

$$\Sigma_{\mathbf{Y-A}} = \sum_i d(\mathrm{TM} - X_i)_{\mathrm{TS}(\mathbf{Y})} - d(\mathrm{TM} - X_i)_{\mathrm{GS}(\mathbf{A})}$$
$$(\mathbf{Y} = \mathbf{B}, \mathbf{D}, \mathbf{E}),$$

where TM is Cr or Mo atom and X represents H and B atoms of the BH_4 moiety. From computed structures, we find a positive value for Σ in all calculations (Table 12). These positive values support an I_d mechanism rather than I_a, which reported earlier [30,33]. This result is consistent with general rule in substitution reactions of organometallic compounds that favors mainly disociative mechanisms [34,35].

4. Conclusion

The main points that this paper put forward can be summarized as follows: (i) In the most stable structure the BH_4 ligand coordinate to TM atom through a η^2 mode, a result that is consistent with the experimental data; (ii) These compounds obey the 18-electron rule; (iii) The mechanisms of hydrogen exchanges, which are an interchange-dissosiative (I_d), pass through the BH_4 twisting about a B–H^t (isomer **E**) or about a B–H^b bond (isomer **B**); (iv) the BH_4 twisting about each B–H bond leads to a η^1 transition state; (v) the BH_4 twisting about B–H^b is more favorable than another case; (vi) In these complexes, the charge transfer from BH_4 ligand to central metal, HOMO–LUMO gap, and the LUMO energy value increase in the order of **A** > **B** = **D** > **E**, indicating that electron donation of BH_4 increases in the order of **A** > **B** = **D** > **E**.

Acknowledgements

The support of SGS cooperation gratefully acknowledged. A. Ariafard thanks Prof. Zhenyang Lin, Dr. Xin Huang and Dr. Siwei Bi, Hong Kong university of Science and Technology, for their fruitful discussion.

References

[1] Z. Xu, Z. Lin, Coord. Chem. Rev. 156 (1996) 139.
[2] A. Lledos, M. Duran, Y. Jean, F. Volatron, Inorg. Chem. 30 (1991) 4440.
[3] P.J. Fischer, V.G.V.G. Young Jr., J.E. Ellis, Angew. Chem., Int. Ed. 39 (2000) 189.
[4] M. Shimoi, S. Nagai, M. Ichikawa, Y. Kaxano, K. Katoh, M. Uruichi, H. Ogino, J. Am. Chem. Soc. 121 (1999) 11704.
[5] D.G. Musaev, K. Morokuma, Organometallics 14 (1995) 3327.
[6] A. Ariafard, R. Fazaeli, H.R. Aghabozorg, J. Mol. Struct. (Theochem) 625 (2003) 305.
[7] Z. Xu, Z. Lin, Inorg. Chem. 35 (1996) 3964.
[8] A. Jarid, A. Lledos, Y. Jean, F. Volatron, Inorg. Chem. 32 (1993) 4695.
[9] J.S. Francisco, I.H. Williams, J. Phys. Chem. 96 (1992) 7567.
[10] T.J. Marks, J.R. Kolb, Chem. Rev. 77 (1977) 263.
[11] M.Y. Darensbourg, R. Bau, M.W. Marks, R.R. Burch Jr., J.C. Deaton, S. Slater, J. Am. Chem. Soc. 104 (1982) 6961.
[12] S.W. Kirtly, M.A. Andres, R. Bau, G.W. Grynkewich, T.J. Marks, D.L. Tipton, B.R. Whittlesey, J. Am. Chem. Soc. 99 (1977) 7154.
[13] A.D. Becke, J. Chem. Phys. 98 (1993) 5648.
[14] C. Lee, W. Yang, R.G. Parr, Phys. Rev. B 37 (1988) 758.
[15] R.G. Parr, W. Yang, Density Functional Theory of Atoms and Molecules, Oxford University Press, New York, 1989.
[16] M.J. Frisch, G.W. Trucks, H.B. Schlegel, G.E. Scuseria, M.A. Robb, J.R. Cheeseman, V.G. Zakrzewski Jr., J.A. Montgomery, R.E. Stratmann, J.C. Burant, S. Dapprich, J.M. Millam, A.D. Daniels, K.N. Kudin, M.C. Strain, O. Farkas, J. Tomasi, V. Barone, M.C.R. Cossi, B. Mennucci, C. Pomelli, C. Adamo, S. Clifford, J. Ochterski, G.A. Petersson, P.Y. Ayala, Q. Cui, K. Morokuma, D.K. Malick, A.D. Rabuck, K. Raghavachari, J.B. Foresman, J. Cioslowski, J.V. Ortiz, A.G. Baboul, B.B. Stefanov, G. Liu, A. Liashenko, P. Piskorz, I. Komaromi, R. Gomperts, R.L. Martin, D.J. Fox, T. Keith, M.A. Al-Laham, C.Y. Peng, A. Nanayakkara, C. Gonzalez, M. Challacombe, P.M.W. Gill, B. Johnson, W. Chen, M.W. Wong, J.L. Andres, C. Gonzalez, M. Head-Gordon, E.S. Replogle, J.A. Pople, GAUSSIAN 98, Revision A.7, Gaussian Inc., Pittsburgh, PA, 1998.
[17] P.J. Hay, W.R. Wadt, J. Chem. Phys. 82 (1985) 299.
[18] J. Andzelm, S. Huzinaga, Gaussian Basis Sets for Molecular Calculation, Elsevier, New York, 1984.

[19] (a) R. Ditchfield, W.J. Hehre, J.A. Pople, Chem. Phys. 54 (1971) 724;
(b) W.J. Hehre, R. Ditchfield, J.A. Pople, J. Chem. Phys. 56 (1972) 2257.
[20] E.D. Glendening, A.E. Read, J.E. Carpenter, F. Weinhold, NBO (Version 3.1), Gaussian Inc., Pittsburgh, PA, 1998.
[21] K.B. Wiberg, Tetrahedron 24 (1968) 1083.
[22] A. Reed, L.A. Curtiss, F. Weinhold, Chem. Rev. 88 (1988) 899.
[23] G. Frenking, N. FrÖhlich, Chem. Rev. 100 (2000) 717.
[24] P.E.M. Siegbahn, in: S.A. Rice, I. Prigogine (Eds.), Advances in Chemical Physics, Wiley, New York, 1996.
[25] S. Niu, M.B. Hall, Chem. Rev. 100 (2000) 353.
[26] M. Mancini, P. Bougeard, R. Burns, M. Mlekuz, B.G. Sayer, J.I.A. Thompson, M.J. McGlinchey, Inorg. Chem. 23 (1984) 1072.
[27] A.J. Downs, R.G. Egdell, A.F. Orchard, P.D.P. Thomas, J. Chem. Soc., Dalton Trans. (1978) 1755.
[28] R.H. Crabtree, Angew. Chem., Int. Ed. 32 (1993) 789.
[29] E.A.V. Ebsworth, D.W.H. Rankin, S. Cradock, Structural Methods in Inorganic Chemistry, Blackwell Scientific Publications, London, 1987.
[30] F. Maseras, A. Lledos, E. Clot, O. Eisenstein, Chem. Rev. 100 (2000) 601.
[31] F. Rotzinger, J. Am. Chem. Soc. 118 (1996) 6760.
[32] I. Ciofini, C. Adamo, J. Phys. Chem. A 105 (2001) 1086.
[33] Y. Oishi, T.A. Albright, H. Fujimoto, Polyhedron 14 (1995) 2603.
[34] J.D. Atwood, Inorganic and Organometallic Reaction Mechanisms, Brooks/cole, Monterey, CA, 1985.
[35] S.-K. Kang, T.A. Albright, C. Mealli, Inorg. Chem. 26 (1987) 3158.